1 **Comparison of water-soluble and insoluble organic compositions attributing to different light**

2 **absorption efficiency between residential coal and biomass burning emissions**

3 Lu Zhang [1,2], Jin Li [1], Yaojie Li[1], Xinlei Liu [1], Zhihan Luo [1], Guofeng Shen [1, *], and Shu Tao [1,3]

4 *1. Laboratory for Earth Surface Process, College of Urban and Environmental Sciences, Peking*

5 *University, Beijing 100871, China*

6 *2. Hong Kong Polytechnic University, Department of Civil & Environmental Engineering,*

7 *Kowloon, Hong Kong, China*

8 *3. College of Environmental Science and Technology, Southern University of Science and*

9 *Technology, Shenzhen 518055, China*

11 ** Corresponding author: Dr. Guofeng Shen, Peking University, Email: gfshen12@pku.edu.cn*

12   **Abstract**

13   There are growing concerns about the climate impacts of absorbing organic carbon (also known as

14   brown carbon, BrC) in the environment, yet its chemical composition and association with the light

15   absorption capabilities remain poorly understood. This study characterized water-soluble and water-

16   insoluble organic carbon (WSOC, WIOC) from residential solid fuel combustion at the molecular

17   level and evaluated their quantitative relationship with mass absorption efficiency (MAE). The

18   MAE values at λ=365 nm from biomass burning were significantly higher than those from coal

19   combustion (p<0.05). Thousands of peaks were identified in the m/z range of 150-800, with the

20   most intense ion peaks occurring between 200-500 m/z for WSOC and 600-800 m/z for WIOC,

21   respectively. The CHO group predominated in WSOC extracts from biomass burning emissions

22   while sulfur-containing compounds (SOCs) including CHOS and CHONS were more intense in the

23   WIOC extracts, particularly from coal emissions. Emissions of the CHON group were positively

24   correlated with the fuel nitrogen content (r=0.936, p<0.05), explaining their higher abundance in

25   coal emissions compared to biomass. The SOCs emissions were more predominant during flaming

26   phases, as indicated by a positive correlation with modified combustion efficiency (MCE) (r=0.750,

27   p<0.05). The unique formulas of coal combustion aerosols were in the lower H/C and O/C regions

28   with higher unsaturated compounds in the van Krevelen (VK) diagram. In WIOC extracts, coal

29   combustion emissions contained significantly higher fractions of condensed aromatics (32-59%),

30   compared to only 4.3-9.7% in biomass burning emissions. In contrast, the CHOS group in biomass

31   burning emissions was characterized by larger condensed aromatic compound fractions than those

32   in coal combustion. Moreover, the CHOS aromatic compound fractions were positively correlated

33   with MAE values in both WSOC (r=0.714, p<0.05) and WIOC extracts (r=0.929, p<0.001),

34   suggesting these compounds significantly contributed to MAE variabilities across different fuels.

Keywords: light absorption properties, atmospheric aerosols, N-containing compounds, S-containing compounds, water-soluble compounds, water-insoluble compounds.

TOC
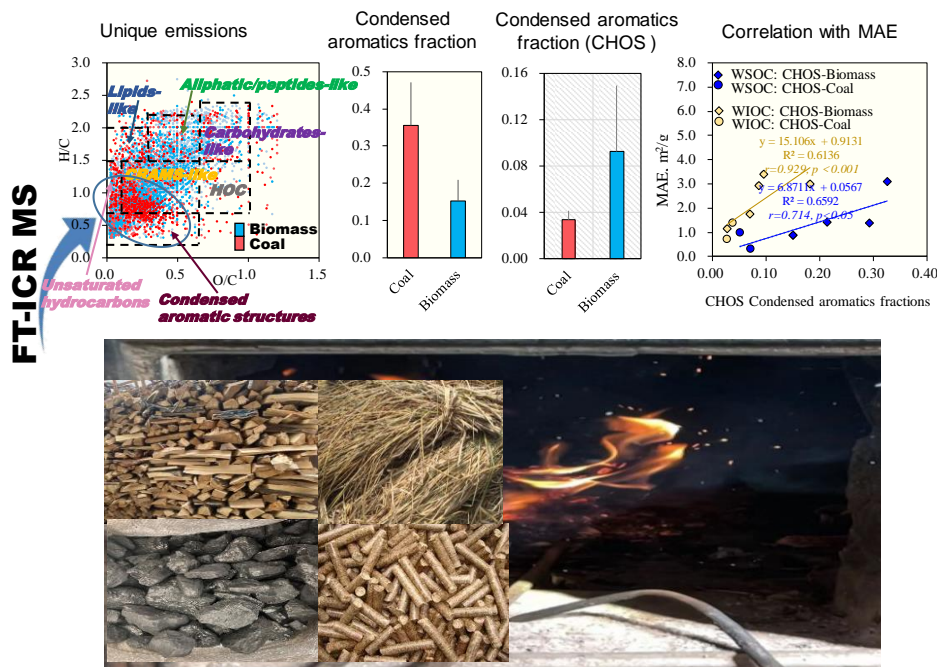
1. Introduction

Light-absorbing organic carbon (OC), known as brown carbon (BrC), attracts growing concerns due to its direct radiative impact on climate change (Laskin et al., 2015; Wang et al., 2022). The global simulations suggested that BrC may contribute nearly 20% of the surface organic aerosol (OA) burden (Jo et al., 2016), and accounted for 19% of the light absorption by anthropogenic aerosols (Feng et al., 2013). BrC originates from diverse sources, including primary emissions from coal combustion, biomass burning, and vehicular emissions (Du et al., 2014; Olson et al., 2015; Bond, 2001; Sun et al., 2017; Chen and Bond, 2010), and secondary processes like the oxidation of volatile organic compounds (Guan et al., 2020; Laskin et al., 2015). Among these sources, residential solid fuel burning produced large amounts of BrC, accounting for 74% of the total anthropogenic primary emissions (Xiong et al., 2022).

49   Some efforts have been made to explore the BrC physiochemical properties in residential

50   emissions. For example, water-soluble organic carbon (WSOC) and methanol-soluble organic

51   carbon (MSOC) were analyzed in primary emissions from combustions of crop straw, wood fuel,

52   and some coals (Park and Yu, 2016). Available studies suggested that the optical properties of

53   primary BrC varied significantly, influenced by numerous factors including inherent fuel properties

54   and combustion conditions. Mass absorption efficiency (MAE) is a key parameter in assessing the

55   direct radiative forcing of light-absorbing carbonaceous aerosols (Huo et al., 2018). It was found

56   that water-soluble BrC derived from bituminous coals had higher MAE values than anthracites

57   (Tang et al., 2020). However, the specific chemical components responsible for the differences in

58   light absorption among various fuel types are not yet fully understood, especially at the molecular

59   level. It was also reported that the mass absorption of water-insoluble organic carbon (WIOC) could

60   be even greater than that of the water-soluble ones (Chen and Bond, 2010; Huang et al., 2018).

61   However, there is limited information available regarding their chemical components. Given the

62   significant variation in BrC light absorption across different fractions emitted from various fuels

63   (Xie et al., 2017), detailed information of a comprehensive characterization, including the chemical

64   and optical characteristics of the BrC fractions (both water-soluble and water-insoluble) from the

65   combustion source, is needed.

66   This study investigated the chemical compositions and light absorption abilities of WSOC and

67   WIOC in smoke particles generated from the burning of coals with different maturity, raw biomass

68   fuels, and biomass pellets in traditional and improved stoves. The use of biomass pellets has been

69   heavily promoted over the last several years to mitigate air pollutant emissions from traditional solid

70   fuels, and emission characteristics from improved stoves could be different from traditional ones.

71   Optical property variations were quantitatively assessed and analyzed to explore their association

72   with chemical components. Furthermore, unique molecules and fingerprints for coal and biomass

73   sources were discussed, which is critical in pollution source appointment.

74   **2.   Materials and methods**

75   2.1 Laboratory combustion emission experiment

76   In the present study, a total of fourteen types of coals with varying maturity degrees, five types

77   of biomass pellets, and twelve types of raw biomass were examined using a laboratory combustion

78   system. Two types of stoves, including a traditional stove (TS) and an improved stove (IS), were

79   utilized for the experiments. The thirty-four fuel-stove combinations are listed in Table S1. The

80   combustion tests were performed in a specially designed system with real-time online monitors

81   (Thermo Scientific Inc., Bremen, Germany), which are capable of continuously measuring gaseous

82   pollutants, including CO, CO_2, hydrocarbons (HC), and nitrogen oxide (NO_X including NO and

83   NO_2). $PM_{2.5}$ (particles with aerodynamic diameters ≤2.5 μm) was collected at a flow rate of 16.7

84   L/min with the quartz filters. Fuel properties including moisture (M_{ad}, %), volatile matter content

85   (V_{daf}, %), ash content (A_{ad}, %), lower heating value (LHV, MJ/kg), and contents of carbon (C, %),

86   hydrogen (H, %), nitrogen (N, %), and sulfur (S, %) are tested, and listed in Table S1. Details of

87   stove construction and combustion processes were available in Zhang et al., (2022).

88   Modified combustion efficiency (MCE) was calculated by integrating the incremental

89   concentrations of CO_2 and CO as:

90         $$MCE = \frac{CO_2}{CO_2 + CO}$$

91   where CO_2 and CO represent the excess molar mixing ratios of CO_2 and CO, respectively

92   (Pokhrel et al., 2016). The MCE values indicate different phases of combustion: approximately 1

93   during flaming, and between 0.7-0.9 during smoldering (Yokelson et al., 1997)

94   2.2 Bulk carbon and UV-vis absorption spectra

95   For each sample, a 4.9 cm^2 filter was extracted ultrasonically with 10 mL Milli-Q water (18.2

96   MΩ) for 30 min, and then the supernatant was separated. The extraction process was repeated twice,

97   and the extracts were combined. The water extract was then filtered via a 0.22 μm

98   polytetrafluoroethylene (PTFE) filter to obtain WSOC. Due to the inefficiency of water in extracting

99   BrC, the insoluble PM components remaining on the sample filter were freeze-dried and subjected

100   to methanol extraction through sonication. The resulting extract was then filtered using a PTFE filter,

101   yielding a water-insoluble fraction referred to as WIOC in the following text. The carbon content

102   of WSOC was analyzed with a total organic carbon (TOC) analyzer (TOC-Lcph/cpn, SHIMADZU,

103   Japan), and the WIOC was determined by subtracting WSOC from the total OC loaded on the same

104   4.9 cm^2 area, given that the methanol extraction efficiency for all combustion samples was up to

105   90% (Zhang et al., 2022). The element carbon (EC) and OC were measured using a thermal-optical

106   analyzer (Sunset OC/EC analyzer) with an interagency monitoring of protected visual environments

107   (IMPROVE) program.

108   The light absorption spectra of the water and methanol extracts were measured between 200

109   nm and 600 nm by UV–vis spectrophotometer (UV-2600, Shimadzu, Japan) at a step size of 1 nm.

110   MAE values of WSOC and WIOC at the wavelength of λ ($MAE_{λ, WSOC}$; $MAE_{λ, WIOC}$) were calculated

111   as following equation (Li et al., 2019):

112   $MAE_{λ, WSOC} = A_{λ, WSOC} × \ln(10)/(C_{WSOC} × L)$; $MAE_{λ, WIOC} = A_{λ, WIOC} × \ln(10)/(C_{WIOC} × L)$

113   where $A_{λ, WSOC}$ and $A_{λ, WIOC}$ is the light absorption value of WSOC extract and WIOC extract

114   at a wavelength of λ, respectively; C is the concentration of WSOC (or WIOC), and L is the optical

115   path length, which is 0.01 m in this study. It is important to note that the reported light absorption

116   of WIOC in this study was underestimated, while such underestimation is insignificant due to the

117   high extraction efficiency. In this study, the MAE values of extractable OC at λ of 365 nm ($MAE_{365,}$

118    $_{WSOC}$ and MAE$_{365, WIOC}$) were discussed.

119   Absorption Ångström exponent (AAE) values were determined based on the following

120   equation (Li et al., 2019; Li et al., 2020):

121    $$A_\lambda = K_\lambda^{-AAE}$$

122   where K is a constant and AAE is obtained through the linear regression of lg (A$_\lambda$) against lg λ

123   (Fig S1). A wavelength of 300-400 nm is chosen according to the published literature (Yue et al.,

124   2022), and the goodness of fit for all the samples in this study is greater than an r^2 of 0.99.

125   2.3 Molecular composition analysis

126   For further molecular composition analysis, the WSOC and WIOC extracts from seven selected

127   source samples were subjected to Fourier-transform ion cyclotron resonance mass spectrometry (FT-

128   ICR MS) coupled with electrospray ionization (ESI). These samples included two types of coals

129   (high volatile bituminous coal, HVB; medium volatile bituminous coal, MVB) combusted in TS,

130   two types of raw biomass (rice straw and pine wood) combusted in TS, pine wood combusted in IS,

131   and two types of biomass pellets (crop straw pellet and pine wood pellet) combusted in IS as noted

132   in SI. FT-ICR MS has been successfully applied for the molecular-level characterization of

133   compounds (Bianco et al., 2018) due to its ultrahigh resolution and mass accuracy. ESI is well-

134   adopted to characterize soluble aerosols, especially for the detection of polar, hydrophilic molecules

135   like humic-like substances (HULIS)-type compounds (Wozniak et al., 2008), because it is a "soft"

136   ionization technique generating minimal analyte fragments, and thus can detect intact molecules of

137   compounds. Therefore, the negative ESI-FT-ICR was applied here to determine the molecular

138   compositions of WSOC and WIOC from combustion samples from different solid fuels. The

139   methanol extracts were evaporated to dryness under a gentle stream of nitrogen and then dissolved

140   with Milli-Q water. The WSOC and water-reconstituted WIOC were submitted to solid-phase

141   extraction (SPE) using Bond Elut PPL (500 mg, 6 mL, Agilent, U.S.A.). Before the extraction, the

142   PPL cartridges were sequentially conditioned with 12 mL methanol and 12 mL Milli-Q water

143   containing 0.05% hydrochloric acid (HCl). The extract was adjusted to pH=2 using HCl to remove

144   inorganic ions and was then loaded onto the PPL cartridges at a rate of 5 mL/min. Cartridges were

145   washed with 18 mL Milli-Q water containing 0.05% HCL to remove salt and then dried under pure

146   nitrogen. Analytes were eluted with 12 mL methanol, and the combined eluates were concentrated

147   to 1 mL. Then the molecular characterization was conducted using a 15T SolariX XR FT-ICR MS

148   (Bruker Daltonik GmbH, Bremen, Germany) in the negative ESI mode. The capillary inlet voltage

149   was set at -4.0 kV and ion accumulation time was set to 0.06 S. There were 300 continuous 4 M

150   data FT-ICR transients added to improve the signal-to-noise ratio. The FT-ICR MS was calibrated

151   with 10 mmol/L sodium formate in advance, and internal standard calibration with soluble organic

152   matter (known molecular formula) was performed after the test. Finally, <1 ppm absolute mass error

153   was achieved. Data processing details are described in the Supporting Information (SI).

154   **3.   Result and discussion**

155   3.1   Optical characteristics of WSOC and WIOC

156   MAE is an important parameter reflecting the light absorption capability of the carbonaceous

157   aerosols. The $MAE_{365,\ WSOC}$ of aerosols from residential sources in this study ranged from 0.21 to

158   3.1 m^2/g with an average of 1.3±0.7 m^2/g. MAE values of extractable OC in this study were lower

159   than that of 11.3 m^2/g for pure BC aerosols (Bond and Bergstrom, 2006) and also lower than that

160   from the filter-based MAE values of OC of 0.16-13 m^2/g from residential sources (Zhang et al.,

161   2021b). A significant difference ($p<0.05$) of $MAE_{365,\ WSOC}$ was observed among the different fuels

162   (Fig.1). The $MAE_{365,\ WSOC}$ of raw biomass combustion derived aerosols averaged at 1.7±0.8 m^2/g,

163   which was significantly higher ($p<0.05$) than those from coal smoke (0.93±0.44 m^2/g) and biomass

164   pellet smoke (1.2±0.6 m^2/g). The MAE$_{365,\ WIOC}$ ranged from 0.49 to 6.6 m^2/g with an average of

165   2.0±1.3 m^2/g. The absorption capability was higher for the WIOC extract than the WSOC extract.

166   This is thought to be associated with distinct chemical compositions of light-absorbing organics. It

167   was noted that the WIOC had higher MAE values compared to the WSOC, which may be explained

168   by the more hydrophobic PAHs and quinones (Chen and Bond, 2010). The difference in MAE$_{365,}$

169    $_{WIOC}$ among the different fuels was also statistically significant (p<0.05), as the value obtained from

170   raw biomass burning (2.8±1.4 m^2/g) was significantly higher than that from coal combustion

171   (1.2±0.6 m^2/g). It was suggested that the MAE values of soluble OC including WSOC and WIOC

172   were dependent on the chemical composition of OC, that is, the chemical structure of the light-

173   absorbing chromophores and the ratio of non-light-absorbing organics to the chromophore

174   components (Cao et al., 2021). The higher MAE values of raw biomass combustion-derived aerosols

175   might be caused by the stronger light absorption capability of chromophores or a higher ratio of

176   chromophores. Our result was comparable to the published data, for example, the MAE$_{365,\ WSOC}$ was

177   reported to average at 1.37±0.23 m^2/g for biomass burning emissions (Park and Yu, 2016). The

178   correlation of MAE with the MCE was investigated. The variability in MAE values, for both WSOC

179   and WIOC, was observed to be negatively correlated with the MCE (or temperature as MCE was

180   found to be positively correlated with the measured temperature in emission exhausts) when pooling

181   all data together as seen in Fig. 1C and 1D. However, within each fuel group, there was no

182   statistically significant correlation between the MAE and MCE values (Fig. S2). Some previous

183   studies found that OC from wood pyrolysis under higher temperature conditions had stronger

184   absorption capability (Chen and Bond, 2010; Saleh et al., 2014), but relatively higher mass

185   absorption coefficient (MAC) values were also reported for the organic aerosol from wood

186   combustion under the 150°C<T<250°C compared to emissions at a lower (T<150°C) or higher

187   (250°C<T<380°C) temperature condition (Rathod et al., 2017). Chen et al., (2010) reported that that

188 absorption per mass (α/ρ) of methanol extracts increased with increased wood pyrolysis temperature,

189 but such increase was nonlinear and varied in burning emissions of different fuel types or wood with

190 different sizes. Therefore, the negative correlations between MAE and MCE values when pooling

191 all data together in Fig. 1 were from distinct absorption properties of emissions from different fuel

192 types, rather than conditions like combustion temperature.

193   The AAE which indicates the wavelength dependence of light absorption is also an important

194 parameter in climate models. The calculated AAE in the WSOC extract (AAE_{WSOC}) ranged from

195 3.8 to 11 with an average of 6.9±1.5, and the difference in AAE_{WSOC} values among the different

196 fuels was statistically significant ($p<0.05$) (Fig.1). The highest values were observed for the aerosols

197 from raw biomass combustion of 7.5±1.4, followed by coal smoke of 6.7±1.5 and biomass pellet

198 smoke of 5.6±1.2. The AAE values in the WIOC extract (AAE_{WIOC}) were slightly lower than

199 AAE_{WSOC}, which ranged from 4.2 to 6.5 with an average of 5.5±0.5. The differences in AAE_{WIOC}

200 values among the different fuels were statistically insignificant ($p>0.05$), with averaged values of

201 5.8±0.3 for coal smoke, 5.1±0.9 for biomass pellet smoke, and 5.2±0.4 for raw biomass smoke.

202 There was a weak positive correlation of AAE_{WIOC} between the MCE values ($p<0.05$). The filter-

203 based analysis also showed that AAE values were positively correlated with MCE values, indicating

204 that more BrC were produced under the smoldering phase compared with BC (Zhang et al., 2020).

205 This study suggested that BrC in WIOC extract was apt to be generated during the smoldering phase

206 in comparison with the non-light-absorbing OC. The AAE values in soluble OC in this study were

207 higher than 4 for all samples, confirming the contribution of BrC to aerosol absorptivity from source

208 emission. The result of this study was comparable to the published literature. For example, it was

209 reported that the AAE_{WSOC} was in the range of 8.6-15 from coal combustion-derived aerosols (Song

210 et al., 2019), and 6.2-9.3 from biomass smoke (Park and Yu, 2016). The AAE_{WIOC} from wintertime

211   urban aerosols were 5.4 ± 0.2 in Xi'an and 5.7 ± 0.2 in Beijing (Huang et al., 2020).
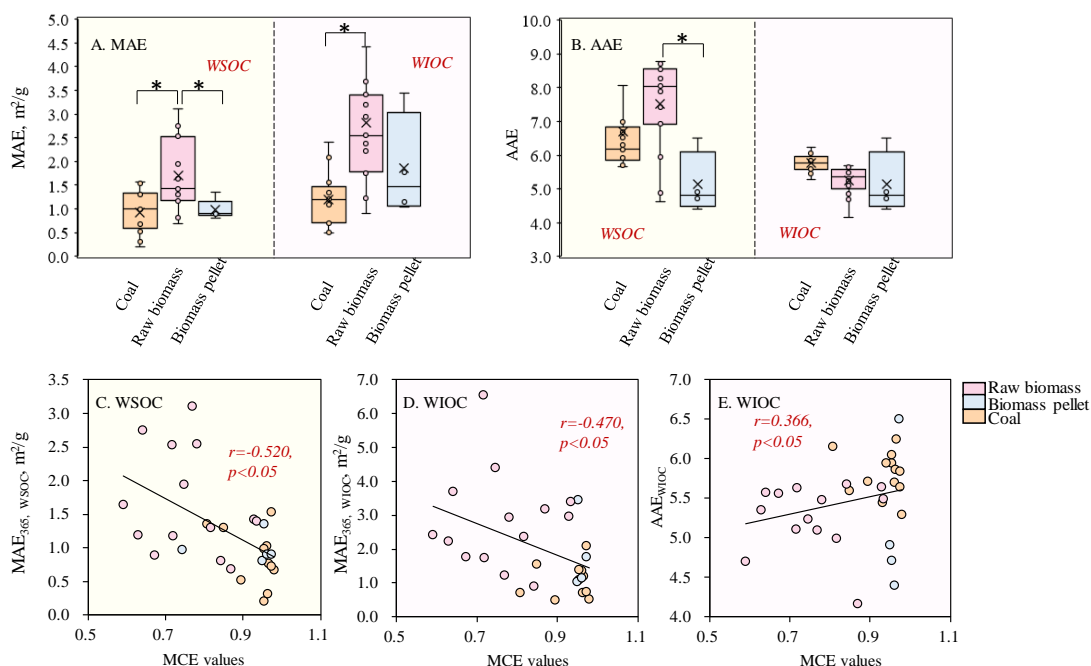
212   **Fig. 1** MAE values at λ=365 nm (A) and AAE values (B) from the source samples (* represents

213    $p<0.05$); Correlation between the MCE values with $MAE_{365, WSOC}$ values (C), $MAE_{365, WIOC}$ values

214   (D), and AAE_{WIOC} values (E).

215   3.2 Molecular characteristics of WSOC and WIOC

216   The ESI-FT-ICR mass spectra of WSOC and WIOC samples are presented in Fig. 2. Thousands

217   of peaks were identified in the m/z range of 150-800, indicating a complex chemical composition

218   of aerosols from residential sources. Formulas detected in the raw biomass burning aerosols were

219   significantly higher than those in biomass pellet and coal smoke (Fig. S3), which indicated a higher

220   chemical complexity of raw biomass emissions. In addition, the combustion of pine wood in the

221   improved stove generated fewer compounds, which was 93% of the peaks identified in the

222   traditional stove (Table S2). The likely less complexity might be due to higher combustion

223   efficiencies and temperature in the improved stove. Generally, higher levels of organic aerosol mass

224   would be emitted during less efficient fuel burning, resulting from prolonged smoldering or

225 incomplete burning (Holder et al., 2016). Our results suggested that corresponding higher chemical

226 complexity was also produced during the incomplete combustion in the traditional stove. The most

227 intense ion peaks were distributed in the 200-500 m/z for WSOC, accounting for 58-86% of the

228 total intensity. Similar results were also found in residential coal combustion (Song et al., 2019),

229 biomass burning (Song et al., 2018), and ambient aerosols (Wozniak et al., 2008).

230 The mass spectra of WIOC are different from the WSOC, especially in aerosol emitted from

231 coal combustion (Fig. 2). WIOC contained more molecules with larger m/z values of 600-800 in

232 range, which indicated that WIOC extract had more compounds with higher molecular weight (MW)

233 than the WSOC extract. According to the molecular formulas and the intensity of each negative ion,

234 the average molecular formulas for the WSOC were obtained with C atom from 20 to 24, H (21-

235 29), N (0.32-0.75), O (5.6-7.0), and S (0.28-0.51) in the WSOC extract. All aerosols from biomass

236 burning, either raw or pelletized ones, had higher relative O atom contents than coal smoke,

237 indicating a higher oxidation degree of biomass emissions. For the WIOC, the average molecular

238 formulas were assigned with 27-33 C, 26-35 H, 0.67-1.2 N, 6.6-11 O, and 0.34-0.92 S. The coal

239 combustion-derived aerosols had more C, N, and S atoms, but less H atom, compared with raw

240 biomass. The combustion of biomass pellets is also assigned with relatively higher S elements. In

241 addition, the WIOC fraction had a higher relative atom content than the corresponding formulas of

242 WSOC from the same source aerosol samples. These results indicated that in addition to the fuel

243 type, extraction solvent also had an important impact on the elemental composition of extractable

244 BrC.
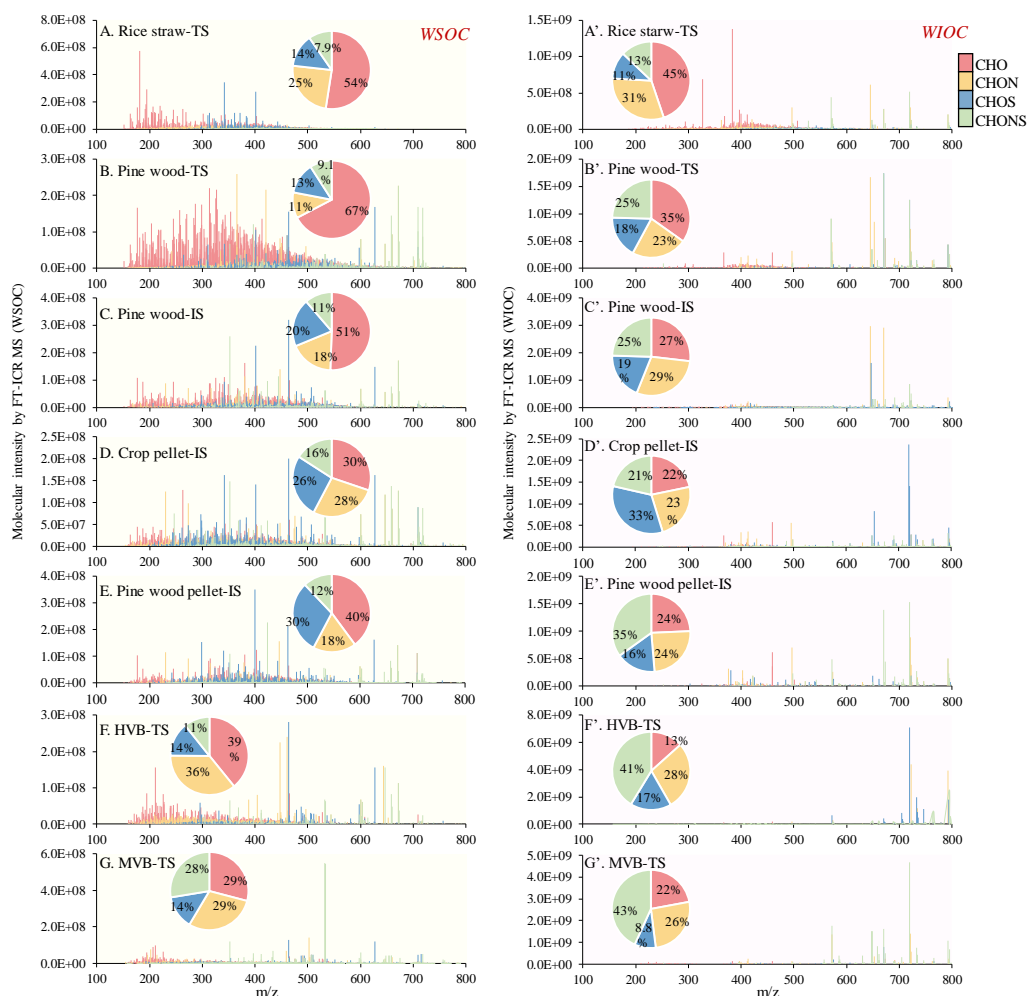
Fig. 2 Negative ESI FT-ICR mass spectra of WSOC (A-G) and WIOC (A'-G') from the seven aerosol samples, TS represents combustion in the traditional stove and IS represents combustion in the improved stove. Different formula groups were color-coded. The pie charts showed the relative intensities of different formula groups.

Molecular formulas identified by the FT-ICR-MS can be classified into 4 groups according to the elemental composition, including CHO (containing only C, H, O), CHON (hereafter similarly), CHOS, and CHONS. CHO was the most abundant group in the WSOC. The CHO group contributed 51-67% to the total intensity of aerosols from raw biomass burning, which were significantly higher than those from biomass pellets (29-39%) and coal smoke (30-40%). The CHO compounds with oxygen-containing functional groups (e.g., hydroxyl, carbonyl, carboxyl, or esters) have been widely identified in both ambient aerosols (Jiang et al., 2021; Mo et al., 2022) and some source

256   samples (Tang et al., 2020). These compounds contributed a broad range of proportions, from 43%

257   to 69% in residential biomass burning smoke (Tang et al., 2020), 9.7-48% in coal smoke (Song et

258   al., 2019), and 20-39% in ambient aerosols (He et al., 2023) for the WSOC extract, which were

259   comparable to ours. CHON compounds were also an important component in the aerosols,

260   accounting for 29-36% of coal smoke, which was significantly higher than biomass burning smoke

261   of 11-28%. One previous study reported that CHON species were more abundant in biomass burning

262   smoke rather than in coal combustion ones (Song et al., 2018). This high fraction of CHON

263   compounds in coal smoke might be caused by the higher nitrogen content of coals as seen in Table

264   S1. A strongly significantly positive correlation was found between the fuel nitrogen content and

265   CHON species percentage (r=0.936, p<0.05) (Fig. 3). Such dependence was also found in the

266   emission factors (EFs) of NO_X on fuel nitrogen content in our result (Fig. S4), as well as NOx, HCN,

267   and NH_3 emissions reported by published literature (Hansson et al., 2004). Sulfur-containing

268   compounds (SOCs; including CHOS and CHONS) abundance was lower than CHO and CHON

269   group, accounting for only 22-42% (13–30% for CHOS and 7.9–28% for CHONS, respectively).

270   The fractions of SOCs in the aerosols from coal combustion (25-42%) and biomass pellet burning

271   (~42%) were comparable but significantly higher than those from raw biomass (22-31%). The

272   abundance of SOCs was not statistically correlated with fuel S content in the present study for

273   pooled data. However, when fuel subgroups were considered, fuels (coal or raw biomass) with

274   higher sulfur content had higher SOCs levels. Also, higher SOCs emission was found for pine wood

275   combusted in the improved stove which have higher combustion efficiency than that in the

276   traditional stove. These results suggested that except for fuel sulfur content, the fuel type and

277   combustion efficiency would also influence the SOCs emissions.

278   In the WIOC, the intensities of these four groups among different source samples were different

279   from those in the WSOC. The CHO group accounted for 27-45% in raw biomass burning aerosols,

280 22-24% in biomass pellet smokes, and 13-22% of coal smokes. On the contrary, the SOCs

281 abundance was significantly higher in WIOC, especially for the coals, accounting for 58% for HVB

282 and 52% for MVB. A significantly positive correlation between the MCE values and SOCs

283 abundance in the WIOC extract was found (r=0.750, $p<0.05$) (Fig. 3), while no clear association

284 between fuel sulfur content and SOCs emissions was observed in the WIOC. Combining the result

285 from the WSOC extract, the strong dependence of SOCs emissions on the combustion conditions

286 was expected, while the fuel sulfur content had a slight influence. Notably, the SOCs abundance in

287 aerosols from coal combustion was greatly higher than that in ambient aerosols (Lin et al., 2012),

288 indicating that residential non-desulfurized coal combustion might be an important emitter of SOCs

289 in atmospheric samples. The CHON group emissions were determined mainly by the fuel nitrogen

290 content, while SOCs emissions were strongly related to the combustion conditions (e.g., flaming

291 phase). It should be noted that the results of our analysis based on the current data without isotopic

292 internal standard used were semi-quantitative, some uncertainties must be addressed.
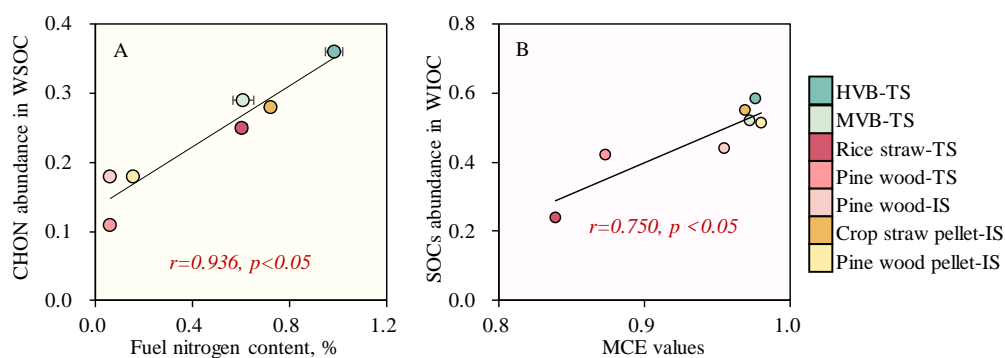
293 **Fig. 3** Correlation between fuel nitrogen contents and abundances of CHON in WSOC (A), and the

294 correlation between MCE values and the abundances of SOCs in WIOC (B). TS represents

295 combustion in the traditional stove and IS represents combustion in the improved stove.

296 3.3 Detailed CHO/CHON/CHOS/CHONS group differences across fuel types

297   Van Krevelen (VK) diagrams which can provide a visual interpretation of complex mass

298 spectra can qualitatively identify chemical composition profiles in mixtures (Lv et al., 2016). The

299 classification criteria of the VK diagram are provided in Table S3 (Patriarca et al., 2018; Tang et al.,

300 2020). Fig. S5 and S6 show the VK diagrams of WSOC and WIOC. In both WSOC and WSOC

301 extract, the carboxylic-rich alicyclic molecules (CRAMs-like) were the most abundant component,

302 contributing to 53-69% in the WSOC extract and 37-56% in the WIOC extract, respectively. The

303 condensed aromatics were also an important component in source samples, accounting for 7.3-13%

304 in the WSOC, and for a higher proportion of 8.6-44% in the WIOC. This observation could be

305 attributed to the hydrophobic property of condensed aromatic hydrocarbons, leading to a lower

306 proportion in the highly polar WSOC. Among the identified formulas, 7.0-13% of total intensity in

307 the WSOC and 3.6-17% in the WIOC were the aliphatic/peptide-like compounds. Such fractions

308 were comparable to unsaturated hydrocarbons with percentages of 3.9-15% in the WSOC and 2.0-

309 11% in the WIOC. The compounds including lipids-like species and highly oxygenated compounds

310 (HOC) were in a relatively lower abundance, with less than 10% each in the source samples. The

311 different fuels showed varied chemical composition characteristics. Coal combustion aerosols had

312 lower H/C ratios than those in biomass burning aerosols, indicating higher unsaturated degrees

313 (Table S2). As indicated by the VK diagrams, the coal combustion produced a notable number of

314 condensed aromatics, contributing to 27%-44% of the WIOC, which was significantly higher than

315 8.6-21% in biomass burning emissions. The modified aromaticity index ($AI_{mod,w}$) which is a

316 measure of aromatic and condensed aromatic structure fractions, and the double bonds equivalent

317 (DBE) values which are used as a measure of the unsaturated level in a molecule were all higher for

318 coal emissions compared to the biomass emissions.

319   Distinct compound profiles being identified by the VK diagram classification criteria are

320 consistent with discrepancies in the four groups (CHO/CHON/CHOS/CHONS). For the CHO group,

321 the most intense compounds were CARMs compounds with fractions of 69-84% in the WSOC

322 extract and higher fractions of 51-80% in the WIOC extract. It was observed that raw biomass would

323   emit slightly more CRAMs (76-84% in the WSOC and 61-80% in the WIOC) than coal (69-73% in

324   the WSOC and 62-69% in the WIOC) and biomass pellet (70-75% in the WSOC and 51-56% in the

325   WIOC) combustion. The condensed aromatic compound was also a crucial component, accounting

326   for 13-20% of the WSOC and 19-27% of the WIOC from coal emissions. These fractions were

327   significantly higher than those found in raw biomass (4.5-10% in the WSOC, 7.9-10% in the WIOC)

328   and biomass pellet (3.8-5.4% in the WSOC, and 11% in the WIOC) (Fig. 4). The other components

329   accounted for a small (less than 10% each) of the total CHO intensity.

330   It was reported that the CHON compounds with $O/N \geq 3$ might be the organonitrates candidate

331   and nitro-substituted compounds, attributing to the allocation of one nitro (NO_2) or nitrooxy (ONO_2)

332   group (Bianco et al., 2018). In this study, the relative content of $CHON_{O/N \geq 3}$ compounds (concerning

333   the overall CHON) in the biomass (raw and pellet ones) ranged between 71-82% and 85-91% for

334   the WSOC and WIOC, which is distinctly lower than those found in coal smokes (86-90% for the

335   WSOC, and 86-95% for the WIOC) (Table S4). Moreover, the $AI_{mod,w}$ values for CHON compounds

336   from coal combustion were higher than the biomass smokes for both WSOC and WIOC, as indicated

337   by Table S2. It can thus be concluded that more CHON compounds with low aromaticity and a large

338   amount of oxidized nitrogen functional groups were formed during the combustion of biomass fuels.

339   Coal combustion emissions had more intense condensed aromatic compounds with a percentage of

340   45-50% for the CHON group, which were significantly higher than those from raw biomass (4.5-

341   37%) and biomass pellet burning (14-30%). This result confirmed the conclusion that the CHON

342   compounds produced from the combustion of coals were characterized by a relatively high

343   aromaticity and a low degree of oxidation.

344   The O-rich CHOS fraction ($O/S \geq 4$) accounted for 42-71% (concerning the overall CHON

345   group) in the WSOC and 45-95% in the WIOC. O-rich CHOS fraction ($O/S \geq 4$) content from coal

346 (66-70% in the WSOC, and 78-98% in the WIOC) and biomass pellet (67-71% in the WSOC, 76-

347 87% in the WIOC) were relatively higher than the raw biomass smoke (42-56% in the WSOC, and

348 32-57% in the WIOC), suggesting that most of the CHOS compounds in coal and pellet smoke can

349 be potentially assigned with more bearing sulfate ($-OSO_3H$) or sulfonate ($-SO_3$) groups. Different

350 from CHO and CHON groups, it was found that the CHOS group in the biomass burning aerosols

351 had a much more intense condensed aromatic structure with a percentage of 14-33% in the WSOC

352 and 2.5-19% in the WIOC, especially for raw biomass (WSOC: 22-33%, WIOC:8.5-19%) than coal

353 combustion (WSOC: 4.9-7.0%, WIOC: 2.5-7.0%). For the CHOS group in the WIOC extract, the

354 unsaturated hydrocarbons were also an important component, accounting for 12-29% of raw

355 biomass burning emissions, which were significantly higher than those in biomass pellet (6.9-11%)

356 and coal (1.5-13%). These results indicated biomass burning emissions were characterized by higher

357 unsaturation levels and aromaticity for the CHOS group than coal combustion.

358   Nearly 34-85% of CHONS formulas have many O atoms ($\geq$7), indicating the existence of the

359 $-NO_3$ group (Table S4). These CHONS compounds are probably nitrooxy-organosulfates (Song et

360 al., 2019). The remaining compounds (15-66%) of the CHONS group had less than 7 atoms,

361 implying that large amounts of CHONS compounds were assigned with reduced N (e.g., amide and

362 nitrile, and heterocyclic aromatics). The condensed aromatic compounds identified by the VK

363 diagram in the WIOC from coal combustion accounted for 22-64%, which was relatively higher

364 than those from biomass burning (14-31%), indicating a higher degree of aromaticity. This was

365 consistent with the difference observed in the $AI_{mod,w}$ values as seen in Table S2. The $AI_{mod,w}$ of

366 WIOC in coal emissions were 0.38 for HVB and 0.60 for MVB, and the values were higher than

367 the raw biomass (0.32-0.38) and biomass pellet (0.35-0.36), confirming a higher aromatic

368 compounds content of coal smoke sample than biomass for CHONS group.

369   Therefore, the CHO, CHON, and CHONS groups generated from coal combustion were

370   characterized by high unsaturated levels with more aromatic species, while CHOS groups had

371   higher aromaticity degrees in biomass smoke aerosols. Aromatic compounds might be the strong

372   BrC chromophores contributing to light absorption (Song et al., 2019). The difference in MAE

373   between coal and biomass emissions and its association with the chemical components will be

374   discussed in detail in section 3.5.
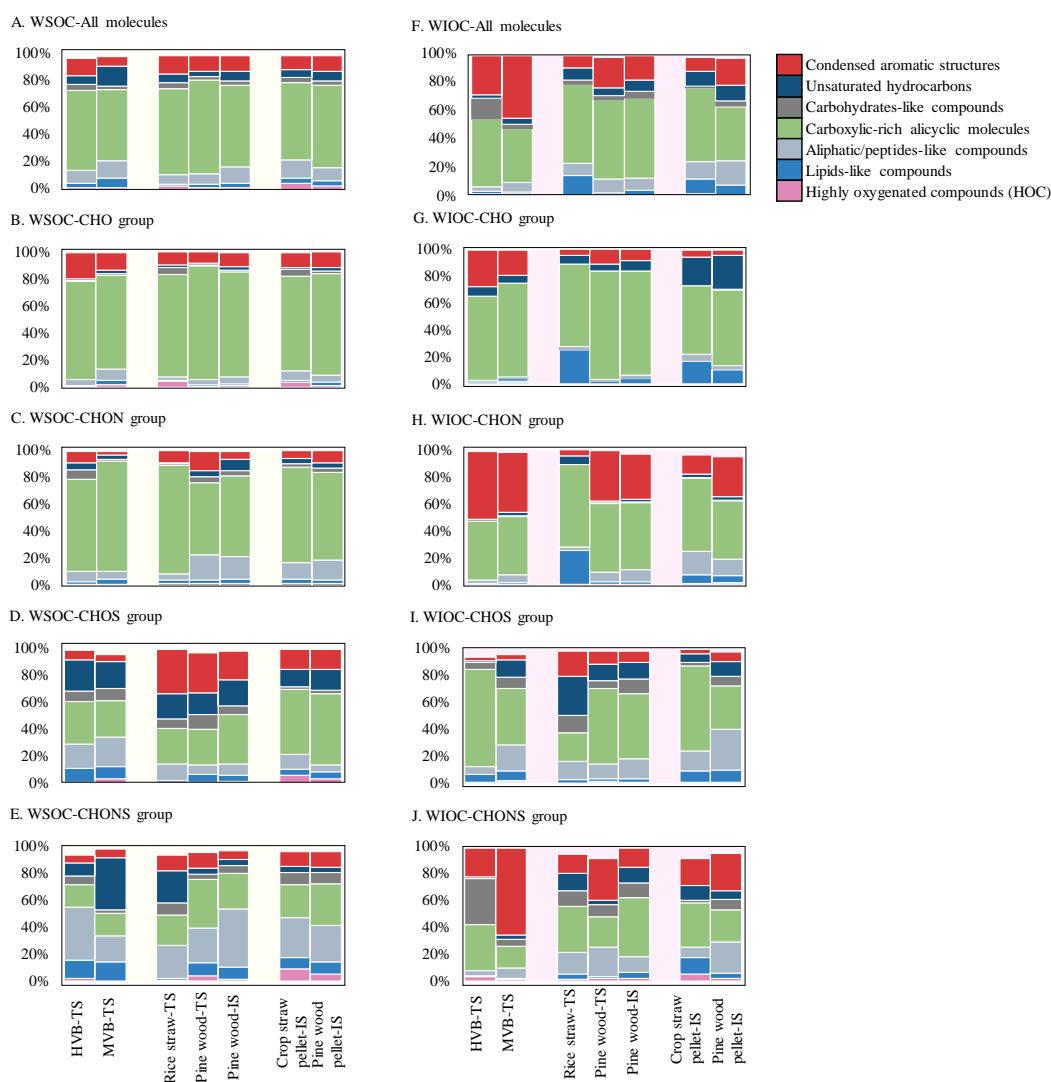
375   **Fig. 4** Each component abundance identified by VK diagram of WSOC (A: all molecules, B: CHO

376   group,   C: CHON group, D: CHOS group, E: CHONS group) and WIOC (F: all molecules, G:

377   CHO group,   H: CHON group, I: CHOS group, J: CHONS group), the classification criteria was

378   provided in the Table S3.

379   3.4 Likely unique molecules of biomass and coal combustion

380   The unique molecules may be inferred from the Venn diagram of formulas as shown in Fig. S7.

381   Among the observed compounds, 3039 and 1624 unique molecular formulas were detected in the

382   combustion of rice straw and pine wood in the traditional stove in the WSOC fractions, which was

383   significantly higher than those found in biomass pellet-improve stove (638-696) and coal-traditional

384   stove (570-734). This suggested a notable difference between the emissions from raw biomass and

385   coal, even when using the same stove. Interestingly, fewer unique peaks were observed for pine

386   wood-improved stoves (533), indicating that using an improved stove for raw biomass could narrow

387   the difference between coal and biomass emissions. A similar trend was also found in the WIOC

388   fractions (Fig. S7). The CHONS group accounted for a significant portion of unique formulas in

389   source samples, particularly in coal smokes, representing 51-52% in WSOC and 51-69% in WIOC

390   extract. The important role of the CHONS group in unique emissions from coal combustion was

391   also noted by Tang et al., (2020), who reported that CHO and CHON were the main components of

392   unique molecular formulas of raw biomass burning emissions among the raw biomass burning, coal

393   combustion and vehicle emissions, representing 88%-93%. This fraction was higher than our result

394   of 33-77% in raw biomass and only 26-27% in biomass pellet. The distribution of the unique

395   molecules further indicated substantial discrepancies among the fuels. Unique molecules in coal

396   combustion-derived aerosols were in the region with lower H/C and O/C values compared with all

397   other samples (Fig. 5) in both WSOC and WIOC extract, indicating a higher degree of unsaturation

398   and lower level of oxidation. For example, it was observed that specific emissions from coal

399   combustion were mainly composed of condensed aromatics (32-59%), followed by CRAMs

400   compounds (23-39%) in WIOC extract. However, only 4.3-9.7% condensed aromatics of the total

401   unique emissions were observed for biomass burning, with CRAMs being the main component (39-

402   65%). As for different groups of CHO/CHON/ CHONS, the condensed aromatic compound contents

403   for all three groups in coal smoke aerosol (unique detected ones) were relatively higher than biomass.

404   While CHOS group showed a different trend in that condensed aromatic compound contents of

405   biomass smoke (unique detected ones) were relatively higher than coal smoke in WSOC extract and

406   comparable to coal smoke in WIOC extract. This finding highlighted the CHOS group's importance

407   in distinguishing the aerosols from the combustion of coals or biomass, helping conduct the source

408   apportionment of aerosols. Additionally, compared with the pine wood-improved stove emissions,

409   most unique molecules in aerosol from pine wood-traditional stove combustion were in the region

410   with lower H/C and O/C ratios (Fig. 5), which were identified mainly as CRAMs compounds. The

411   emissions from the improved stove were distributed in a wider range with fewer CRAMs

412   compounds and more aliphatic/peptides-like compounds observed. Unique molecules from biomass

413   pellets combusted in the improved stove distributed in the upper region of the VK diagram with

414   higher H/C values in WIOC extract, which indicated a lower unsaturated degree (Fig. S8).

415
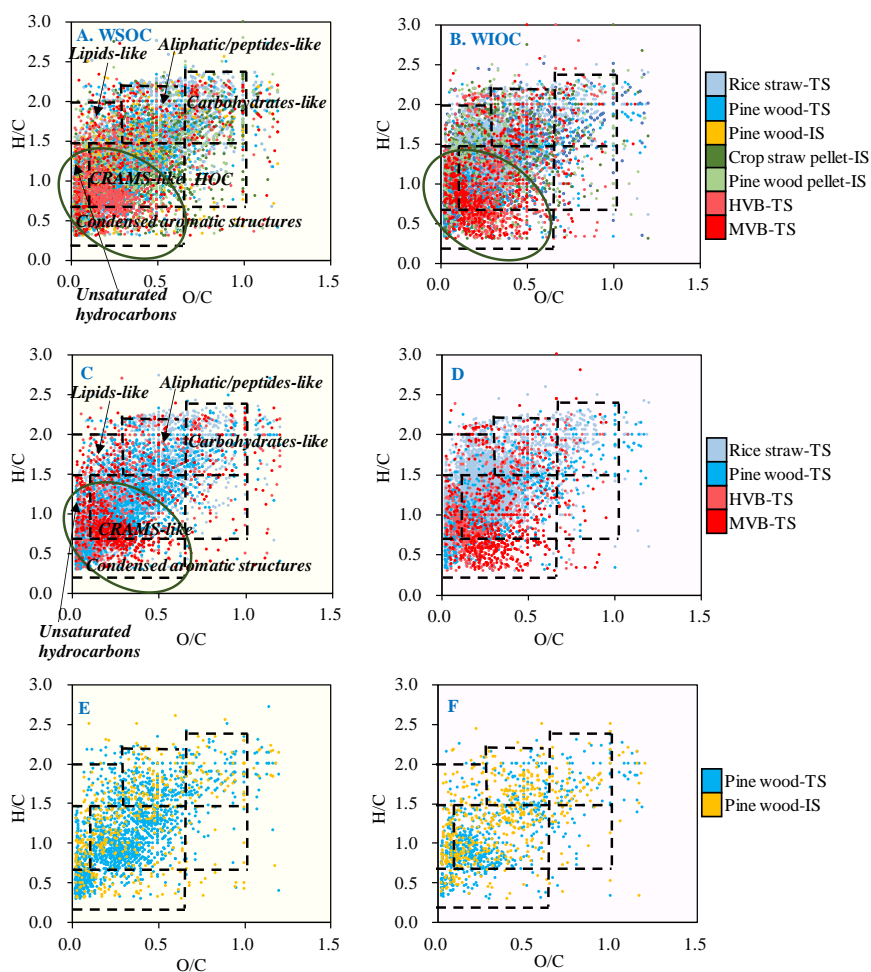
416   **Fig. 5** Van Krevelen diagrams of WSOC (left) and WIOC (right) from the source samples, TS

417   represents combustion in the traditional stove and IS represents combustion in the improved stove.

418   Different color indicates unique formulas detected in each sample of solid fuel combustion.

419   A total of 484 molecular formulas were detected simultaneously in the seven aerosol samples

420   in the WSOC extract and 306 in the WIOC extract. Among these commonly detected molecules,

421   most of which were CHO compounds with the molecular numbers accounting for 60% and 73% in

422   the WSOC and WIOC, respectively. CHON accounted for 31% of WSOC and 19% of WIOC, while

423   SOCs only occupied about 10%. As seen in Fig. S9, these CHO compounds were mainly composed

424   of CRAMs-like compounds and several lipids-like and aliphatic/peptides-like compounds.

425   Moreover, these compounds were relatively small molecular compounds assigned with 8-28 C

426   atoms and 2-12 O atoms with DBE values of 2-17 for the WSOC extract. The relatively more C

atom assigned with larger DBE values was observed for the CHO compounds in WIOC, which

could be partially explained by that the overall CHO compounds in the WIOC extract had larger

MW values with a high degree of unsaturation. In total, the CHON compounds were also CRAMs-

like compounds, and almost none compounds were expected to be aromatics. CHOS and CHONS

species had much fewer formulas, especially for CHONS, only accounting for 1.0% of the

commonly detected molecules in the WIOC. The unsaturated levels of commonly detected

molecules in all seven source samples were relatively low. For example, the condensed aromatic

compounds accounted for 6.5-9.3% and 3.3-4.1% of the total intensity for coal smoke and biomass

smoke in the WSOC, respectively, as well as 0.38-8.3% and 18-21% in the WIOC extract. Different

from the CHO, CHON, and CHONS groups, high percentages of condensed aromatic compounds

were found in the CHOS group (commonly detected ones) from raw biomass burning aerosols with

a range of 6.6-51% in the WSOC and 12-46% in the WIOC extract. These fractions were

significantly higher than those from coal smokes of 4.1-4.9% in the WSOC and 8.8-25% in the

WIOC extract. Combining the finding that the CHOS group in biomass smokes had a higher

aromaticity degree in both WSOC and WIOC extract. However, the unique molecules in WIOC

extract did not follow this trend. It was thus speculated that the higher aromaticity degree of the

CHOS group in biomass smokes was attributed to the intensity variation of these simultaneously

detected compounds, rather than the unique emission from a special source for the WIOC extract.

To explore the potential influence of fuel properties and combustion conditions on chemical

composition, the major factors such as fuel moisture, V_{daf}, and parameters reflecting combustion

conditions including MCE, and EC/OC ratios were assessed. The linear correlation analysis was

applied to estimate the effect of these factors on each molecular intensity (commonly detected ones)

(Fig.S10 and S11). The aliphatic compounds (including lipids-like, aliphatic/peptides-like, and

carbohydrates-like compounds) were negatively correlated with the fuel moisture and positively

451 correlated with V_{daf} and EC/OC ratios. Fuel moisture has been recognized as an important factor

452 influencing pollutant formation, but the influence is usually very complicated. The observed

453 relationship between fuel water content and pollutant EFs varies largely among studies, which may

454 be attributed to factors such as different water contents, pollutant types, and interactions among

455 other influencing factors. Fuels with high moisture levels may have high emissions, as extra energy

456 is needed to vaporize water during the burning process; however, a decrease in combustion

457 temperatures under very high-water content conditions may slow the pollutant formation rate and

458 consequently lower emissions. Higher EC/OC ratios and larger MCE values tend to be associated

459 with stronger flaming conditions. The results suggested that the aliphatic compounds were apt to be

460 produced during the period of the flaming phase with higher combustion temperature. This result

461 could partially explain that aliphatic/peptides-like compounds would be apt to be produced in the

462 improved stove rather than the traditional stove. In comparison, the emissions of CRAMs-like

463 compounds which are the most abundant species were decreased with the increased MCE and

464 EC/OC values, indicating that CARMs-like compounds were generated under the smoking phase.

465 No significant correlations of aromatics, unsaturated hydrocarbons, and HOCs were observed with

466 these parameters, resulting from their small proportion in commonly detected molecules. It is worth

467 noting that there may be significant differences, even for the same fuel, in chemical composition

468 depending on other factors such as stove type and combustion conditions. The interactions among

469 these factors make it difficult to assess their influence. It was found that only around 50% of

470 identified molecules were overlapped emissions for pine wood combusted in the traditional stove

471 and in the improved stove, suggesting the importance of the stove used. A smaller fraction of 25-

472 30% molecules were observed compared to the pine wood emissions with coals combusted in the

473 same stove, which suggested that the influence of varied fuels on chemical composition could

474 surpass the differences caused by different stoves. Our previous studies have revealed that fuel type

475 was the most important factor influencing the MAE values (Zhang et al., 2021b) and BrC EFs

476 (Zhang et al., 2021a). The present study highlighted the dominant effect of fuel type on the chemical

477 composition of soluble OC, providing a theoretical basis for source appointment based on molecular

478 composition. Moreover, the combustion conditions would have a significant effect on the molecular

479 intensity, resulting in differences in MAE eventually as indicated in section 3.1.

480 3.5 The correlation of light absorption properties with molecular compositions

481 Here we specifically investigate the variability in optical characteristics among the different

482 fuels attributed to their chemical compositions. No significant correlations were observed between

483 the AAE values of soluble OC and the molecular composition, indicating that AAE could be

484 influenced by many factors. The MAE may be influenced by the degree of oxidation and

485 unsaturation degree (Mo et al., 2017) (Tang et al., 2020), however, there was no significant

486 correlation found between the MAE values and O/C values in the present source samples, implying

487 that the BrC light absorption ability might not be directly affected by its oxidation degree.

488 The $MAE_{365, WSOC}$ values were significantly positively correlated with the DBE values (r=0.786,

489 $p<0.05$) and the MW values (r=0.750, $p<0.05$) (Fig. S12), indicating that unsaturation and MW

490 played a crucial role in the light absorption capability of the source samples. In the above discussion,

491 we have noticed that the CHOS group in biomass was characterized by a higher degree of

492 aromaticity than coal smoke aerosol, while the CHO, CHON, and CHONS groups have a higher

493 aromatic degree in the coal emissions. A significantly positive correlation (r=0.714, $p<0.05$) was

494 observed between $MAE_{365, WSOC}$ values, and the condensed aromatics percentages from the CHOS

495 group (Fig. 6), indicating that aromatics in the CHOS group contributed to the high light absorption

496 ability of biomass smokes.

497 For the WIOC extract, no significant correlation was found between the $MAE_{365, WIOC}$ values

with MW or DBE values, which might be explained by much different chemical composition for insoluble compounds compared with soluble parts Although the coal combustion emitted much more aromatic compounds with higher DBE values for the WIOC, the MAE values were not significantly higher. The significantly positive correlation (r=0.929, $p<0.05$) between MAE$_{365,\,WIOC}$ values, and the CHOS condensed aromatics percentages confirmed the importance of CHOS aromatics in determining the light absorption capability from source samples. As mentioned in Section 3.4, the higher aromaticity degree of the CHOS group in biomass smoke was largely due to the intensity variation of these commonly detected compounds in all source samples. Further analysis revealed that MAE$_{365,\,WIOC}$ values were positively correlated (r=0.750, $p<0.05$) with the CHOS condensed aromatics fractions which were the fraction simultaneously detected in all samples. These results indicated that the light absorption capability of source aerosols may be due to the higher abundance of some CHOS aromatic compounds commonly emitted from both coal and biomass, rather than the unique tracers.
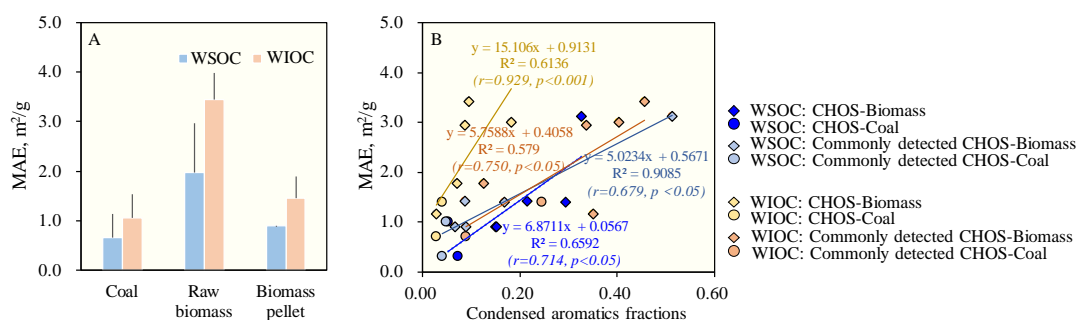
Fig. 6 MAE values at λ=365 nm (A) and correlations between MAE values and condensed aromatics fractions in CHOS and in commonly detected CHOS (B) from the source samples

4. Conclusion and implication

The MAE$_{365,\,WSOC}$ ranged from 0.21 to 3.1 m^2/g with an average of 1.3±0.7 m^2/g. The MAE$_{365,\,WIOC}$ was found to be higher with an average of 2.0±1.3 m^2/g. There were significant differences ($p<0.05$) observed among the different fuels for both MAE$_{365,\,WSOC}$ and MAE$_{365,\,WIOC}$, as raw

517   biomass burning combustion had significantly higher values than the coal combustion. The

518   AAE_{WSOC} ranged from 3.8 to 11 with an average of 6.9±1.5. The AAE_{WIOC} was slightly lower than

519   AAE_{WSOC}, which ranged from 4.2 to 6.5 with an average of 5.5±0.5. Thousands of peaks were

520   identified in the m/z range of 150-800, indicating a complex chemical composition of aerosols from

521   residential sources. CHO group was the most abundant component in the WSOC extracts and the

522   contribution of CHO compounds to the total intensity in aerosols from raw biomass burning was

523   significantly higher than those from biomass pellets and coal smoke. On the other hand, WIOC

524   extract contained more SOCs, especially in the coal combustion aerosol. Notably, CHON

525   compounds were more abundant in the coal combustion emissions, which was due to the higher fuel

526   N content of coals (r=0.936, $p<0.05$). The SOCs emissions were more predominant during flaming

527   phases, with a positive correlation between SOCs abundance with the MCE values (r=0.750,

528    $p<0.05$). The CHO, CHON, and CHONS groups generated from coal combustion were

529   characterized by high unsaturated levels with more aromatic species, while CHOS groups had

530   higher aromaticity degrees in biomass smoke aerosols. It was found that MAE values were

531   positively correlated with the CHOS condensed aromatics proportion for both WSOC (r=0.714,

532    $p<0.05$) and WIOC extract (r=0.929, $p<0.001$). These results indicated that higher CHOS condense

533   aromatics abundance in biomass burning aerosols could partly explain the higher MAE values of

534   raw biomass smoke. Further analysis showed a positive correlation of MAE with the CHOS

535   condensed aromatics fractions which were the fractions simultaneously detected in all samples.

536   These results indicated that the light absorption capability of source aerosols may be due to the

537   higher abundance of some CHOS aromatic compounds commonly emitted from both coal and

538   biomass burning, rather than the unique tracers. The unique formulas of coal combustion aerosols

539   were in the lower H/C and O/C regions with higher unsaturated compounds in the VK diagram. This

540   work is potentially applicable to the source appointment based on the molecular characteristics and

541 to future studies developing more scientific control measures by focusing on one major component

542 (e.g., CHOS condensed aromatics) of light absorption aerosols.

543   There are still some questions that need to be investigated in the future study. First, the study on

544 BrC composition in this research used dissolved OC as a substitute. However, this substitute cannot

545 fully represent BrC emissions. Both WSOC and WIOC contain some non-light-absorbing

546 components, and the proportion of these components is unknown, making it difficult to measure the

547 representativeness of extractable OC for BrC. Additionally, the lack of study about the emissions

548 characteristics under controlled combustion conditions limits the obtained results. Controlled

549 experiments including flaming or smoldering burns, airflow, and combustion temperature are

550 needed in future work. Third, fresh burning-derived OC released into the atmosphere can undergo

551 various aging reactions such as photochemical degradation. These reactions can significantly alter

552 the light absorptivity and chemical properties of BrC components. It is essential to consider the

553 optical properties and lifetimes of organic compounds emitted from solid fuel combustion in climate

554 models.

555 **Data availability.**

556 Data are available by contacting the corresponding authors

557 **Supplement**

558 The following information is in the appendix and available via the Internet:

559   Data processing in the ESI FT-ICR MS; fuel properties of coal and biomass fuels tested;

560 number of formulas in each group, values of elemental ratios, MW, and DBE values in the WSOC

561 and WIOC for each source type; stoichiometric ranges of VK classes; correlation between fuel N

562 and emission factors of NO_X; the VK diagrams of WSOC and WIOC for different source samples;

563   and correlations between the VK plots of WSOC/WIOC and fuel properties or combustion

564   conditions.

Author contributions

566   LZ, GS, and ST designed the experiment. LZ and JL prepared the filters used. LZ, YL, XL and

567   ZL conducted the sample collection. LZ and JL performed the data analysis. LZ wrote the paper.

568   GS, and ST reviewed and commented on the paper.

Competing interests

570   The authors declare that they have no conflict of interest.

Acknowledgment

572   Funding for this study was partly from the National Natural Science Foundation of China

573   (42077328, and 41922057). The authors greatly appreciated the valuable help in data analysis by

574   Prof. Jianzhong Song from CAS.

Financial support

576   This research has been supported by the National Natural Science Foundation of China

577   (42077328, and 41922057)

References

579   Bianco, A., Deguillaume, L., Vaitilingom, M., Nicol, E., Baray, J.L., Chaumerliac, N., and
580   Bridoux, M.: Molecular Characterization of Cloud Water Samples Collected at the Puy de Dome
581   (France) by Fourier Transform Ion Cyclotron Resonance Mass Spectrometry, Environ. Sci. Technol.,
582   52, 10275-10285, https://doi.org/10.1021/acs.est.8b01964, 2018.

583   Bond, T. C.: Spectral dependence of visible light absorption by carbonaceous particles emitted
584   from coal combustion, Geophys. Res. Lett., 28, 4075-4078, https://doi.org/10.1029/2001GL013652,
585   2001.

586   Bond, T. C. and Bergstrom, R. W.: Light absorption by carbonaceous particles: An investigative
587   review, Aerosol Sci. Technol., 40, 27-67, https://doi.org/10.1080/02786820500421521, 2006.

588   Brege, M., Paglione, M., Gilardoni, S., Decesari, S., Facchini, M. C., and Mazzoleni, L. R.:
589   Molecular insights on aging and aqueous-phase processing from ambient biomass burning

emissions-influenced Po Valley fog and aerosol, Atmos. Chem. Phys., 18, 13197-13214, https://doi.org/10.5194/acp-18-13197-2018, 2018.

Burling, I. R., Yokelson, R. J., Griffith, D. W. T., Johnson, T. J., Veres, P., Roberts, J. M., Warneke, C., Urbanski, S. P., Reardon, J., Weise, D. R., Hao, W. M., and de Gouw, J.: Laboratory measurements of trace gas emissions from biomass burning of fuel types from the southeastern and southwestern United States, Atmos. Chem. Phys., 10, https://doi.org/10.5194/acp-10-11115-2010, 2010.

Cao, T., Li, M., Zou, C., Fan, X., Song, J., Jia, W., Yu, C., Yu, Z., and Peng, P.: Chemical composition, optical properties, and oxidative potential of water- and methanol-soluble organic compounds emitted from the combustion of biomass materials and coal, Atmos. Chem. Phys., 21, 13187-13205, https://doi.org/10.5194/acp-21-13187-2021, 2021.

Chen, Y. and Bond, T. C.: Light absorption by organic carbon from wood combustion, Atmos. Chem. Phys., 10, 1773-1787, https://doi.org/10.5194/acp-10-1773-2010, 2010.

Du, Z., He, K., Cheng, Y., Duan, F., Ma, Y., Liu, J., Zhang, X., Zheng, M., and Weber, R.: A yearlong study of water-soluble organic carbon in Beijing II: Light absorption properties, Atmos. Environ., 89, 235-241, https://doi.org/10.1016/j.atmosenv.2014.02.022, 2014.

Fan, X., Li, M., Cao, T., Cheng, C., Li, F., Xie, Y., Wei, S., Song, J., and Peng, P. a.: Optical properties and oxidative potential of water-and alkaline-soluble brown carbon in smoke particles emitted from laboratory simulated biomass burning, Atmos. Environ., 194, 48-57, https://doi.org/10.1016/j.atmosenv.2018.09.025, 2018.

Feng, Y., Ramanathan, V., and Kotamarthi, V. R.: Brown carbon: a significant atmospheric absorber of solar radiation? Atmos. Chem. Phys., 13, 8607-8621, https://doi.org/10.5194/acp-13-8607-2013, 2013.

Hansson, K. M., Samuelsson, J., Tullin, C., and Amand, L. E.: Formation of HNCO, HCN, and NH3 from the pyrolysis of bark and nitrogen-containing model compounds, Combust. Flame, 137, 265-277, https://doi.org/10.1016/j.combustflame.2004.01.005, 2004.

He, T., Wu, Y., Wang, D., Cai, J., Song, J., Yu, Z., Zeng, X., and Peng, P. a.: Molecular compositions and optical properties of water-soluble brown carbon during the autumn and winter in Guangzhou, China, Atmos. Environ., 296, https://doi.org/10.1016/j.atmosenv.2022.119573, 2023.

Holder, A. L., Hagler, G. S. W., Aurell, J., Hays, M. D., and Gullett, B. K.: Particulate matter and black carbon optical properties and emission factors from prescribed fires in the southeastern United States, J. Geophys. Res.: Atmos., 121, 3465-3483, https://doi.org/10.1002/2015JD024321, 2016.

Huang, R.J., Yang, L., Cao, J., Chen, Y., Chen, Q., Li, Y., Duan, J., Zhu, C., Dai, W., Wang, K., Lin, C., Ni, H., Corbin, J. C., Wu, Y., Zhang, R., Tie, X., Hoffmann, T., O'Dowd, C., and Dusek, U.: Brown Carbon Aerosol in Urban Xi'an, Northwest China: The Composition and Light Absorption Properties, Environ. Sci. Technol., 52, 6825-6833, https://doi.org/10.1021/acs.est.8b02386, 2018.

Huang, R.J., Yang, L., Shen, J., Yuan, W., Gong, Y., Guo, J., Cao, W., Duan, J., Ni, H., Zhu, C., Dai, W., Li, Y., Chen, Y., Chen, Q., Wu, Y., Zhang, R., Dusek, U., O'Dowd, C., and Hoffmann, T.: Water-Insoluble Organics Dominate Brown Carbon in Wintertime Urban Aerosol of China: Chemical Characteristics and Optical Properties, Environ. Sci. Technol., 54, 7836-7847, https://doi.org/10.1021/acs.est.0c01149, 2020.

Huo, Y., Li, M., Jiang, M., and Qi, W.: Light absorption properties of HULIS in primary particulate matter produced by crop straw combustion under different moisture contents and stacking modes, Atmos. Environ., 191, 490-499, https://doi.org/10.1016/j.atmosenv.2018.08.038, 2018.

Jen, C. N., Hatch, L. E., Selimovic, V., Yokelson, R. J., Weber, R., Fernandez, A. E., Kreisberg, N. M., Barsanti, K. C., and Goldstein, A. H.: Speciated and total emission factors of particulate

organics from burning western US wildland fuels and their dependence on combustion efficiency, Atmos. Chem. Phys., 19, 1013-1026, https://doi.org/10.5194/acp-19-1013-2019, 2019.

Jiang, B., Kuang, B. Y., Liang, Y., Zhang, J., Huang, X. H. H., Xu, C., Yu, J. Z., and Shi, Q.: Molecular composition of urban organic aerosols on clear and hazy days in Beijing: a comparative study using FT-ICR MS, Environ. Chem., 13, 888-901, https://doi.org/10.1071/EN15230, 2016.

Jiang, H., Li, J., Sun, R., Tian, C., Tang, J., Jiang, B., Liao, Y., Chen, C.-E., and Zhang, G.: Molecular Dynamics and Light Absorption Properties of Atmospheric Dissolved Organic Matter, Environ. Sci. Technol., 55, 10268-10279, https://doi.org/10.1021/acs.est.1c01770, 2021.

Jo, D. S., Park, R. J., Lee, S., Kim, S.-W., and Zhang, X.: A global simulation of brown carbon: implications for photochemistry and direct radiative effect, Atmos. Chem. Phys., 16, 3413-3432, https://doi.org/10.5194/acp-16-3413-2016, 2016.

Laskin, A., Laskin, J., and Nizkorodov, S. A.: Chemistry of Atmospheric Brown Carbon, Chem. Rev., 115, 4335-4382, https://doi.org/10.1021/cr5006167, 2015.

Laskin, A., Smith, J. S., and Laskin, J.: Molecular Characterization of Nitrogen-Containing Organic Compounds in Biomass Burning Aerosols Using High-Resolution Mass Spectrometry, Environ. Sci. Technol., 43, 3764-3771, https://doi.org/10.1021/es803456n, 2009.

Li, J., Zhang, Q., Wang, G., Li, J., Wu, C., Liu, L., Wang, J., Jiang, W., Li, L., Ho, K. F., and Cao, J.: Optical properties and molecular compositions of water-soluble and water-insoluble brown carbon (BrC) aerosols in northwest China, Atmos. Chem. Phys., 20, 4889-4904, https://doi.org/10.5194/acp-20-4889-2020, 2020.

Li, M., Fan, X., Zhu, M., Zou, C., Song, J., Wei, S., Jia, W., and Peng, P. a.: Abundance and Light Absorption Properties of Brown Carbon Emitted from Residential Coal Combustion in China, Environ. Sci. Technol., 53, 595-603, https://doi.org/10.1021/acs.est.8b05630, 2019.

Lin, P., Rincon, A. G., Kalberer, M., and Yu, J. Z.: Elemental Composition of HULIS in the Pearl River Delta Region, China: Results Inferred from Positive and Negative Electrospray High Resolution Mass Spectrometric Data, Environ. Sci. Technol., 46, 7454-7462, https://doi.org/10.1021/es300285d, 2012.

Lv, J., Zhang, S., Wang, S., Luo, L., Cao, D., and Christie, P.: Molecular-Scale Investigation with ESI-FT-ICR-MS on Fractionation of Dissolved Organic Matter Induced by Adsorption on Iron Oxyhydroxides, Environ. Sci. Technol., 50, 2328-2336, https://doi.org/10.1021/acs.est.5b04996, 2016.

McMeeking, G. R., Kreidenweis, S. M., Baker, S., Carrico, C. M., Chow, J. C., Collett, J. L., Jr., Hao, W. M., Holden, A. S., Kirchstetter, T. W., Malm, W. C., Moosmueller, H., Sullivan, A. P., and Wold, C. E.: Emissions of trace gases and aerosols during the open combustion of biomass in the laboratory, J. Geophys. Res.: Atmos., 114, https://doi.org/10.1029/2009JD011836, 2009.

Mo, Y., Li, J., Liu, J., Zhong, G., Cheng, Z., Tian, C., Chen, Y., and Zhang, G.: The influence of solvent and pH on determination of the light absorption properties of water-soluble brown carbon, Atmos. Environ., 161, 90-98, https://doi.org/10.1016/j.atmosenv.2017.04.037, 2017.

Mo, Y., Zhong, G., Li, J., Liu, X., Jiang, H., Tang, J., Jiang, B., Liao, Y., Cheng, Z., and Zhang, G.: The Sources, Molecular Compositions, and Light Absorption Properties of Water-Soluble Organic Carbon in Marine Aerosols From South China Sea to the Eastern Indian Ocean, J. Geophys. Res.: Atmos., 127, https://doi.org/10.1029/2021JD036168, 2022.

Olson, M. R., Garcia, M. V., Robinson, M. A., Van Rooy, P., Dietenberger, M. A., Bergin, M., and Schauer, J. J.: Investigation of black and brown carbon multiple-wavelength-dependent light absorption from biomass and fossil fuel combustion source emissions, J. Geophys. Res.: Atmos., 120, 6682-6697, https://doi.org/10.1002/2014JD022970, 2015.

Park, S. S. and Yu, J.: Chemical and light absorption properties of humic-like substances from

685 biomass burning emissions under controlled combustion experiments, Atmos. Environ., 136, 114-
686 122, https://doi.org/10.1016/j.atmosenv.2016.04.022, 2016.

687 Patriarca, C., Bergquist, J., Sjoberg, P. J. R., Tranvik, L., and Hawkes, J. A.: Online HPLC-
688 ESI-HRMS Method for the Analysis and Comparison of Different Dissolved Organic Matter
689 Samples, Environ. Sci. Technol., 52, 2091-2099, https://doi.org/10.1021/acs.est.7b04508, 2018.

690 Pokhrel, R. P., Wagner, N. L., Langridge, J. M., Lack, D. A., Jayarathne, T., Stone, E. A.,
691 Stockwell, C. E., Yokelson, R. J., and Murphy, S. M.: Parameterization of single-scattering albedo
692 (SSA) and absorption Angstrom exponent (AAE) with EC / OC for aerosol emissions from biomass
693 burning, Atmos. Chem. Phys., 16, 9549-9561, 10.5194/acp-16-9549-2016, 2016.

694 Rathod, T., Sahu, S. K., Tiwari, M., Yousaf, A., Bhangare, R. C., and Pandit, G. G.: Light
695 Absorbing Properties of Brown Carbon Generated from Pyrolytic Combustion of Household
696 Biofuels, Aerosol Air Qual. Res., 17, 108-116, 10.4209/aaqr.2015.11.0639, 2017.

697 Reisen, F., Meyer, C. P., Weston, C. J., and Volkova, L.: Ground-Based Field Measurements of
698 PM2.5 Emission Factors From Flaming and Smoldering Combustion in Eucalypt Forests, J.
699 Geophys. Res.: Atmos., 123, 8301-8314, https://doi.org/10.1029/2018JD028488, 2018.

700 Ren, Q. and Zhao, C.: Evolution of fuel-N in gas phase during biomass pyrolysis, Renewable
701 Sustainable Energy Rev., 50, 408-418, https://doi.org/10.1016/j.rser.2015.05.043, 2015.

702 Saleh, R., Robinson, E. S., Tkacik, D. S., Ahern, A. T., Liu, S., Aiken, A. C., Sullivan, R. C.,
703 Presto, A. A., Dubey, M. K., Yokelson, R. J., Donahue, N. M., and Robinson, A. L.: Brownness of
704 organics in aerosols from biomass burning linked to their black carbon content, Nat. Geosci., 7, 647-
705 650, 10.1038/ngeo2220, 2014.

706 Song, J., Li, M., Jiang, B., Wei, S., Fan, X., and Peng, P. a.: Molecular Characterization of
707 Water-Soluble Humic like Substances in Smoke Particles Emitted from Combustion of Biomass
708 Materials and Coal Using Ultrahigh-Resolution Electrospray Ionization Fourier Transform Ion
709 Cyclotron Resonance Mass Spectrometry, Environ. Sci. Technol., 52, 2575-2585,
710 https://doi.org/10.1021/acs.est.7b06126, 2018.

711 Song, J., Li, M., Fan, X., Zou, C., Zhu, M., Jiang, B., Yu, Z., Jia, W., Liao, Y., and Peng, P. a.:
712 Molecular Characterization of Water- and Methanol-Soluble Organic Compounds Emitted from
713 Residential Coal Combustion Using Ultrahigh-Resolution Electrospray Ionization Fourier
714 Transform Ion Cyclotron Resonance Mass Spectrometry, Environ. Sci. Technol., 53, 13607-13617,
715 https://doi.org/10.1021/acs.est.9b04331, 2019.

716 Sun, J. Z., Zhi, G. R., Hitzenberger, R., Chen, Y. J., Tian, C. G., Zhang, Y. Y., Feng, Y. L.,
717 Cheng, M. M., Zhang, Y. Z., Cai, J., Chen, F., Qiu, Y., Jiang, Z., Li, J., Zhang, G., and Mo, Y.:
718 Emission factors and light absorption properties of brown carbon from household coal combustion
719 in China, Atmos. Chem. Phys., 17, 4769-4780, https://doi.org/10.5194/acp-17-4769-2017, 2017.

720 Tang, J., Li, J., Su, T., Han, Y., Mo, Y., Jiang, H., Cui, M., Jiang, B., Chen, Y., Tang, J., Song,
721 J., Peng, P. a., and Zhang, G.: Molecular compositions and optical properties of dissolved brown
722 carbon in biomass burning, coal combustion, and vehicle emission aerosols illuminated by
723 excitation-emission matrix spectroscopy and Fourier transform ion cyclotron resonance mass
724 spectrometry analysis, Atmos. Chem. Phys., 20, 2513-2532, https://doi.org/10.5194/acp-20-2513-
725 2020, 2020.

726 Wang, Q. Q., Zhou, Y. Y., Ma, N., Zhu, Y., Zhao, X. C., Zhu, S. W., Tao, J. C., Hong, J., Wu,
727 W. J., Cheng, Y. F., and Su, H.: Review of Brown Carbon Aerosols in China: Pollution Level, Optical
728 Properties, and Emissions, J. Geophys. Res.: Atmos., 127, https://doi.org/10.1029/2021JD035473,
729 2022.

730 Wei, W., Xie, Q., Yan, Q., Hu, W., Chen, S., Su, S., Zhang, D., Wu, L., Huang, S., Zhong, S.,
731 Deng, J., Yang, T., Li, J., Pan, X., Wang, Z., Sun, Y., Kong, S., and Fu, P.: Dwindling aromatic
732 compounds in fine aerosols from chunk coal to honeycomb briquette combustion,   Sci.   Total

733 Environ., 838, https://doi.org/10.1016/j.scitotenv.2022.155971, 2022.

734 Wozniak, A. S., Bauer, J. E., Sleighter, R. L., Dickhut, R. M., and Hatcher, P. G.: Technical
735 Note: Molecular characterization of aerosol-derived water soluble organic carbon using ultrahigh
736 resolution electrospray ionization Fourier transform ion cyclotron resonance mass spectrometry,
737 Atmos. Chem. Phys., 8, 5099-5111, https://doi.org/10.5194/acp-8-5099-2008, 2008.

738 Xie, M. J., Hays, M. D., and Holder, A. L.: Light-absorbing organic carbon from prescribed
739 and laboratory biomass burning and gasoline vehicle emissions, Sci. Rep., 7,
740 https://doi.org/10.1038/s41598-017-06981-8, 2017.

741 Xiong, R., Li, J., Zhang, Y., Zhang, L., Jiang, K., Zheng, H., Kong, S., Shen, H., Cheng, H.,
742 Shen, G., and Tao, S.: Global brown carbon emissions from combustion sources, Environ. Sci.
743 Ecotechnology, 12, 100201, https://doi.org/10.1016/j.ese.2022.100201, 2022.

744 Yokelson, R. J., Susott, R., Ward, D. E., Reardon, J., and Griffith, D. W. T.: Emissions from
745 smoldering combustion of biomass measured by open-path Fourier transform infrared spectroscopy,
746 J. Geophys. Res.: Atmos.,, 102, 18865-18877, 10.1029/97jd00852, 1997.

747 Yue, S., Zhu, J., Chen, S., Xie, Q., Li, W., Li, L., Ren, H., Su, S., Li, P., Ma, H., Fan, Y., Cheng,
748 B., Wu, L., Deng, J., Hu, W., Ren, L., Wei, L., Zhao, W., Tian, Y., Pan, X., Sun, Y., Wang, Z., Wu,
749 F., Liu, C.-Q., Su, H., Penner, J. E., Poschl, U., Andreae, M. O., Cheng, Y., and Fu, P.: Brown carbon
750 from biomass burning imposes strong circum-Arctic warming, One Earth, 5, 293-304,
751 https://doi.org/10.1016/j.oneear.2022.02.006, 2022.

752 Zhang, L., Luo, Z., Du, W., Li, G., Shen, G., Cheng, H., and Tao, S.: Light absorption properties
753 and absorption emission factors for indoor biomass burning, Environ. Pollut., 267,
754 https://doi.org/10.1016/j.envpol.2020.115652, 2020.

755 Zhang, L., Luo, Z. H., Li, Y. J., Chen, Y. C., Du, W., Li, G., Cheng, H. F., Shen, G. F., and Tao,
756 S.: Optically Measured Black and Particulate Brown Carbon Emission Factors from Real-World
757 Residential Combustion Predominantly Affected by Fuel Differences, Environ. Sci. Technol., 55,
758 169-178, https://doi.org/10.1021/acs.est.0c04784, 2021a.

759 Zhang, L., Luo, Z., Xiong, R., Liu, X., Li, Y., Du, W., Chen, Y., Pan, B., Cheng, H., Shen, G.,
760 and Tao, S.: Mass Absorption Efficiency of Black Carbon from Residential Solid Fuel Combustion
761 and Its Association with Carbonaceous Fractions, Environ. Sci. Technol., 55, 10662-10671,
762 https://doi.org/10.1021/acs.est.1c02689, 2021b.

763 Zhang, L., Hu, B., Liu, X., Luo, Z., Xing, R., Li, Y., Xiong, R., Li, G., Cheng, H., Lu, Q., Shen,
764 G., and Tao, S.: Variabilities in Primary N-Containing Aromatic Compound Emissions from
765 Residential Solid Fuel Combustion and Implications for Source Tracers, Environ. Sci. Technol.,
766 https://doi.org/10.1021/acs.est.2c03000, 2022.

767 Zhao, Y., Hallar, A. G., and Mazzoleni, L. R.: Atmospheric organic matter in clouds: exact
768 masses and molecular formula identification using ultrahigh-resolution FT-ICR mass spectrometry,
769 Atmos. Chem. Phys., 13, 12343-12362, https://doi.org/10.5194/acp-13-12343-2013, 2013.

770

771